Rate Coefficients and Kinetic Isotope Effect for the C_2H Reactions with NH_3 and ND_3 in the 104−294 K Temperature Range

Boris Nizamov and Stephen R. Leone*

Departments of Chemistry and Physics and Lawrence Berkeley National Laboratory, University of California, Berkeley, California 94720

Received: December 31, 2003; In Final Form: March 1, 2004

Reactions of C_2H with NH_3 and ND_3 are studied at low temperature using a pulsed Laval nozzle apparatus. The C_2H radical is prepared by 193 nm photolysis of acetylene, and the C_2H concentration is monitored using $CH(A^2\Delta)$ chemiluminescence from the $C_2H + O_2$ reaction. The rate constants for the $C_2H + NH_3$ and $C_2H + ND_3$ reactions are measured at three temperatures, 104 ± 5 K, 165 ± 15 K, and 296 ± 2 K. Measured rate constants are fit to power law expressions, $k(T) = A(T/298)^n$, for ease of comparison with the results for the related $CN + NH_3$ reaction and to emphasize the importance of the attractive part of intermolecular interaction potential in the reaction mechanism. The rate constants are $(2.9 \pm 0.7) \times 10^{-11} \times (T/298\ \mathrm{K})^{(-0.90 \pm 0.15)}$ cm^3 molecule^{-1} s^{-1} and $(1.1 \pm 0.2) \times 10^{-11} \times (T/298\ \mathrm{K})^{(-0.82 \pm 0.026)}$ cm^3 molecule^{-1} s^{-1} for NH_3 and ND_3, respectively. A large kinetic isotope effect is observed, $k(C_2H + NH_3)/k(C_2H + ND_3) = 2.0 \pm 0.2$, which within experimental uncertainty does not depend on the temperature in the 104−296 K range. Previous theoretical work shows that a hydrogen abstraction channel, $C_2H + NH_3 \rightarrow C_2H_2 + NH_2$, is a possible mechanism for the $C_2H + NH_3$ reaction since the minimum energy path for this channel does not have an activation barrier. This theoretical prediction is consistent with the strong negative temperature dependence of the rate coefficients for the $C_2H + NH_3$ reaction observed in this work, which clearly shows that the $C_2H + NH_3$ reaction does not have a barrier.

1. Introduction

Reactions of the ethynyl radical (C_2H) play an important role in a wide variety of environments, such as the photochemistry of the outer planets and Titan,[1,2] interstellar chemistry,[3−6] and combustion.[7,8] Laboratory studies of the low-temperature gas-phase chemical reactions involving the C_2H radical are motivated by the practical need for accurate rate constants, which are required for the photochemical models of planetary atmospheres, as well as by the desire for a better understanding of the reaction mechanisms, which can be achieved by studying reactions over as wide a range of temperatures as possible. The $C_2H + NH_3$ reaction may be an important reaction in the photochemistry of the outer planets considering that ammonia and acetylene, which is the C_2H precursor, are significant constituents of the atmospheres of Saturn and Jupiter.[9] Since acetylene and ammonia are also among the most abundant molecules observed in interstellar clouds, and since the rate constants of the $C_2H + NH_3$ reaction are likely to be large at low temperatures (10−50 K), because the results of this work show that the reaction does not have a barrier and the rate constant for this reaction has a negative temperature dependence, one can expect that the $C_2H + NH_3$ reaction may be important in the chemistry of dense interstellar clouds. More general interest in the C_2H reactions at low temperatures arises from the consideration that reactions at low collision energies are sensitive to the properties of the entrance channel, and new information about the long-range part of the potential energy surface (PES) can be obtained from low-temperature kinetics studies. The dynamics of reactions at low-temperature offer intriguing differences from room-temperature mechanisms, including long-lived collisions, attractive potential surfaces, and tunneling.

The photochemistry of Jupiter's upper troposphere, where both acetylene and ammonia are present, was discussed by Kaye and Strobel[10] in relation to the detection of HCN by Tokunaga et al.[11] It should be noted that the upper limit of the HCN mixing ratio in Jupiter was later revised.[12] To explain the production of HCN, Kaye and Strobel[10] proposed that NH_2 radicals produced from NH_3 photolysis might react with unsaturated hydrocarbons such as C_2H_2 and C_2H_3 to eventually form HCN. If the branching ratio for the addition/elimination channel of the $C_2H + NH_3$ reaction is not too small, the $C_2H + NH_3$ reaction can also contribute to the coupling of the carbon and nitrogen chemistries in the atmospheres of Jupiter and Saturn. A general overview of Jupiter's photochemistry can be found in Moses et al.[13]

The reaction of C_2H with NH_3 can proceed via a hydrogen abstraction mechanism (R1), an addition/elimination mechanism (R2), and the formation of an adduct in the presence of collisions, which will stabilize the adduct (R3):

$$C_2H + NH_3 \rightarrow C_2H_2 + NH_2 \quad \Delta H^\circ_{298K} = -121\ \mathrm{kJ/mol} \qquad \text{(R1)}$$

$$\rightarrow HCCNH_3 \rightarrow \text{products} \quad \Delta H^\circ_{298K} < 0 \qquad \text{(R2)}$$

$$\rightarrow C_2H_4N \quad \Delta H^\circ_{298K} < 0 \qquad \text{(R3)}$$

There are many possible products of the $C_2H + NH_3$ reaction and to our knowledge no measurements of product branching ratios have been made. The reverse reaction of R1, $C_2H_2 + NH_2$, has been studied both experimentally[14] and theoretically.[15] The value of ΔH°_{298} for R1 is taken to be equal to the zero

* Corresponding author. Address: Department of Chemistry, University of California, Berkeley, CA 94720. Telephone: 510-643-5467. Fax: 510-642-6262. E-mail: srl@cchem.berkeley.edu.

10.1021/jp031361e CCC: $27.50
Published on Web 03/31/2004

point energy-corrected energy difference between the reactants and the products, which was calculated in the theoretical study.[15] The theoretical study shows that on the minimum energy path from the $C_2H + NH_3$ reactants to the $C_2H_2 + NH_2$ products there is an attractive well, the bottom of which is 11.08 kJ/mol lower than the asymptotic energy of the reactants, followed by a barrier (see Figure 2 of ref 15). The barrier height is calculated to be 4.55 kJ/mol below the asymptotic energy of the reactants (4.15 kJ/mol when adjusted for the zero point energy), which means that the abstraction channel does not have an activation energy. Unfortunately, there are no theoretical studies of the reaction path for the addition/elimination channel, R2, which would allow comparison of the relative importance of R1 and R2. As indicated above, in the addition/elimination channel a new CN bond is formed, followed by a unimolecular reaction, which can result in many products. For example, formation of the new bond can lead to elimination of the hydrogen atom, followed and/or preceded by hydrogen atom rearrangements, finally producing one of the C_2H_3N isomers and a hydrogen atom as products. There are numerous possible isomers of C_2H_3N, and the equilibrium geometries and energies of some of the possible C_2H_3N isomer products can be found in the theoretical study of the $NH_2 + C_2H_2$ reaction.[15] Similarly, for R3 all the possible adducts are denoted as C_2H_4N.

In the present work, the $C_2H + NH_3$ and ND_3 reactions are studied by measuring the temperature dependences of the low-temperature rate coefficients. Surprisingly, there are no previous measurements for the $C_2H + NH_3$ reaction rate constants. Since the CN radical is isoelectronic with the C_2H radical, the $C_2H + NH_3$ reaction is compared to the previously studied $CN + NH_3$ reaction.[16] The results from this work for the $C_2H + NH_3$ reaction are also compared to the results from a previous investigation of the $CH + NH_3$ reaction.[17]

2. Experimental Section

A detailed description of the experiment has been given previously and only a brief overview will be presented here.[18] A Laval nozzle block is mounted on a translational stage inside a vacuum chamber, which is pumped by a mechanical pump (pumping speed ~60 L/s). Low temperatures (165 and 104 K) are produced by supersonic expansion of the gas through low Mach number (*Ma*) $Ma = 2$ and $Ma = 3$ Laval nozzles, respectively. The gas admitted into the chamber through the Laval nozzle block is mainly nitrogen, with small amounts of acetylene, oxygen, and NH_3 or ND_3 reactant. The supersonic expansion is formed by opening a pair of solenoid valves in a preexpansion chamber for ~5 ms. The expansion through the Laval nozzle results in a collimated supersonic gas flow, which has uniform density and temperature distributions. The background pressure is adjusted using a gate valve to obtain the best collimation of the flow. Three milliseconds after the valves are opened, an initial concentration of the C_2H radical is produced by 193 nm photolysis of acetylene using an excimer laser. Typical photolysis fluences inside the vacuum chamber are ~30 mJ/cm^2 in an approximately 10 ns pulse. The laser beam is coaxial with the supersonic flow. Photolysis produces a uniform distribution of the initial C_2H concentration along the length of the supersonic expansion, which is monitored using the chemiluminescence tracer method, by adding oxygen to the gas flow. In this method, the concentration of C_2H is followed in time by observing CH $A(^2\Delta) \rightarrow X(^2\Pi)$ chemiluminescence produced by the $C_2H + O_2$ reaction. The chemiluminescence signal is detected using a photomultiplier tube with a 430 nm band-pass filter (10 nm band-pass) and recorded using a multichannel scaler in a photon counting regime. Typically, a radical decay profile is obtained by accumulating signal from 6000 photolysis laser pulses. Time delays for the opening of the pulsed valves, the pulsing of the excimer laser, and the multichannel scaler trigger are generated using a multiple channel digital delay generator. The experiment is run at a 10 Hz repetition rate.

The temperature of the supersonic expansion is determined by recording the laser-induced fluorescence rotational spectrum of the OH A−X electronic transition. Fluorescence is excited via the A $^2\Sigma^+$ ($v' = 1$) ← X $^2\Pi$ ($v'' = 0$) transition using the frequency doubled output of a dye laser pumped by a frequency doubled Nd:YAG laser and detected via the A $^2\Sigma^+$ ($v' = 1$) ← X $^2\Pi$ ($v'' = 1$) transition using a band-pass filter. The temperature was determined by plotting the natural logarithm of the intensities of the OH A $^2\Sigma^+$ ($v' = 1$) ← X $^2\Pi$ ($v'' = 0$) rotational lines divided by the degeneracy of the lower rotational states vs the lower rotational state energies. More details about the determination of the temperature in the Laval nozzle supersonic expansion can be found in an earlier report.[19]

The total gas density is calculated using the measured background pressure in the chamber (which is equal to the pressure in the supersonic expansion) and the temperature of the expansion. The concentration of the reactant is calculated from the total gas density in the supersonic expansion (the total density is typically $(2.1 \pm 0.2) \times 10^{16}$ cm^{-3} for the $Ma = 3$ nozzle and $(5.7 \pm 0.7) \times 10^{16}$ cm^{-3} for the $Ma = 2$ nozzle) and the flow rates of the carrier gas, acetylene, oxygen and the reactant (ammonia or deuterated ammonia), which are monitored using flow meters. The concentrations of O_2 and C_2H_2 in the supersonic expansion are similar to the concentrations used in a previous study.[20] The purities of gases are as follows: N_2, 99.999%; C_2H_2, 99.6%; O_2, 99.998%; NH_3, 99.999%; ND_3, 99.9%. Since acetylene is stabilized by acetone, it is purified further by passing it through an activated carbon filter. For room temperature measurements, the gas mixture is continuously flowed into the chamber through a port in one of the flanges, bypassing the Laval nozzle block.

3. Results

Rate constants are measured under pseudo-first-order conditions where the concentration of the reagent is much larger than the C_2H concentration. The kinetics of C_2H removal under these conditions can be expressed as

$$-\mathrm{d}[C_2H]/\mathrm{d}t = [C_2H](k[R] + k_{oxygen}[O_2] + k_{acetylene}[C_2H_2]) = k_{obs}[C_2H] \quad (1)$$

where R is the ammonia reagent and k is the rate constant for the $C_2H + R$ reaction. The bimolecular rate constants, k, are determined by plotting the observed first-order decay rate constants, k_{obs}, vs the reagent concentration, [R].

Chemiluminescence from the electronically excited $CH(A^2\Delta)$ radical produced in the C_2H reaction with O_2 is used to follow the C_2H concentration in time. Details of the 193 nm photolysis of C_2H_2 to create an initial concentration of C_2H radical and the chemiluminescence tracer method are discussed previously.[21] Under the conditions of our experiment, the chemiluminescence signal is proportional to the C_2H concentration. Typical decay traces of the chemiluminescence signal are shown in Figure 1. The two traces shown in Figure 1 correspond to two different concentrations of the reactant, while all the other experimental parameters are kept constant. As can be seen, the plots of the natural logarithm of the signal vs time are linear, confirming

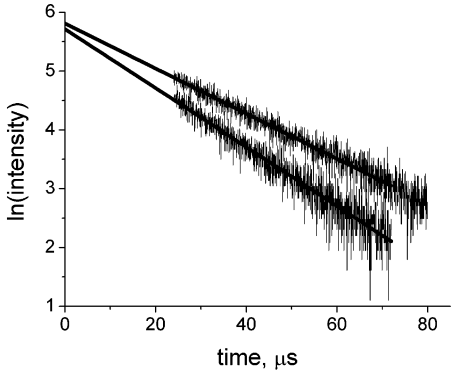

Figure 1. Plot of the natural logarithm of the CH A → X 0−0 chemiluminescence signal vs time. The upper and lower traces are collected for $[ND_3] = 1.8 \times 10^{14}$ cm^{-3} and $[ND_3] = 7.6 \times 10^{14}$ cm^{-3}, respectively, $T = 296 \pm 2$ K, and $(7.1 \pm 0.3) \times 10^{16}$ cm^{-3} total gas density. The intercepts from extrapolation of the chemiluminescence signal to time equal zero are very close, and the small difference in the intercept values may indicate a slight difference in the quenching of the CH A → X 0−0 chemiluminescence signal by the reactant.

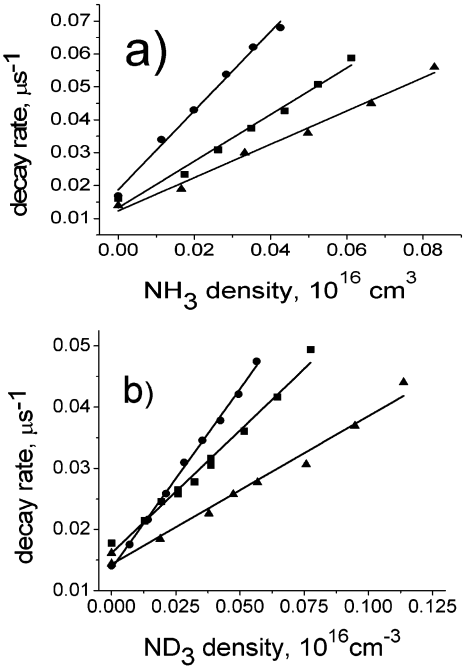

Figure 2. (a) Plot of the first-order decay rate constants vs the reactant concentration for the C_2H reaction with NH_3 at $T = 104$ K (●), $T = 165$ K (■), and $T = 296$ K (▲). For clarity, the points for the $T = 165$ K and $T = 296$ K plots are shifted by subtracting 0.01 and 0.02 μs^{-1}, respectively. The straight lines are least-squares fits to the experimental points. (b) Plot of the first-order decay rate constants vs the reactant concentration for the C_2H reaction with ND_3 at $T = 104$ K (●), $T = 165$ K (■), and $T = 296$ K (▲). For clarity, the points for the $T = 165$ K and $T = 296$ K plots are shifted by subtracting 0.01 and 0.02 μs^{-1}, respectively. The straight lines are least-squares fits to the experimental points.

that the experiment is done under pseudo-first-order conditions and that the initial concentration of C_2H is uniform along the flow axis. First-order decay rate constants, k_{obs}, are determined from plots like the ones shown in Figure 1 by linear least-squares fitting. Fitting is done starting at 25 μs delay after the photolysis laser pulse to avoid interference from the scattered laser light and emission produced by the photolysis pulse. Figure 2 shows plots of the first-order decay constants vs the reactant concentration for the C_2H reaction with NH_3 and ND_3 at 104, 165, and 296 K. The slopes of the lines give the corresponding bimolecular rate constants, k, for NH_3 and ND_3. The intercept of the first-order rate constant vs the reactant concentration plot is mainly due to C_2H reactions with acetylene and oxygen and, to a lesser extent, due to the diffusion of C_2H radicals out of the irradiated zone.

TABLE 1: Rate Constants[a] for the C_2H Reactions with NH_3 and ND_3

reactant	temp, K	total gas density, 10^{16} cm^{-3}	[reactant], 10^{14} cm^{-3}	rate constant 10^{-10} cm^3 molecule^{-1} s^{-1}
NH_3	104 ± 5	2.1 ± 0.2	0−4	1.20 ± 0.24
	165 ± 15	5.7 ± 0.7	0−6	0.71 ± 0.14
	296 ± 2	7.7 ± 0.4	0−8	0.51 ± 0.09
ND_3	104 ± 5	2.1 ± 0.2	0−5	0.58 ± 0.12
	165 ± 15	5.7 ± 0.7	0−7	0.42 ± 0.08
	296 ± 2	7.1 ± 0.3	0−11	0.24 ± 0.05

[a] The indicated uncertainties are represented as $\pm 2\sigma$, where σ is the standard deviation uncertainty.

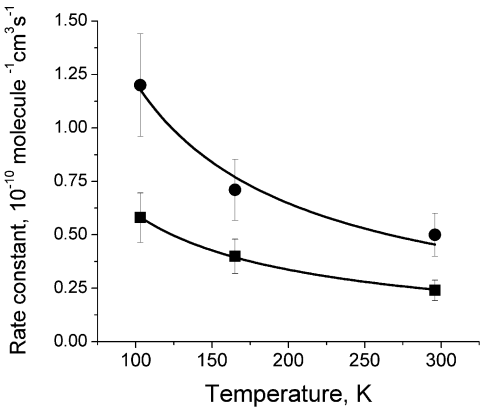

Figure 3. Plot of the rate constants for the C_2H reactions with NH_3 (●) and ND_3 (■) vs the temperature. The fits of the rate constants to power law expressions, $A \times (T/298\text{ K})^n$, give $(2.9 \pm 0.7) \times 10^{-11} \times (T/298\text{ K})^{(-0.90\pm0.15)}$ cm^3 molecule^{-1} s^{-1} and $(1.1 \pm 0.2) \times 10^{-11} \times (T/298\text{ K})^{(-0.82\pm0.026)}$ cm^3 molecule^{-1} s^{-1} for NH_3 and ND_3, respectively.

The measured rate constants are summarized in Table 1, along with the uncertainties, which are reported as 2σ. The indicated uncertainties of the rate constants include both the statistical errors and the uncertainty associated with the inhomogeneity of the gas density and temperature profile along the flow axis. The statistical errors for the rate constants of the C_2H reactions with NH_3 and ND_3 are small, <5%, and the rate constants given in Table 1 are the averages of two measurements. The temperature dependences of the rate constants for the $C_2H + NH_3$ and $C_2H + ND_3$ reactions are shown in Figure 3, and from the dramatic increase with lower temperature it is clear that both reactions do not have a significant energy barrier. For ease of comparison of the rate constants for the $C_2H + NH_3/ND_3$ reactions to the rate constants for the related $CN + NH_3$ reaction, the rate constants for the $C_2H + NH_3/ND_3$ reactions are fit to the $k(T) = A(T/298\text{ K})^n$ form. As noted in one study of low-temperature gas-phase kinetics, this form is often more appropriate than an Arrhenius form with a negative activation energy to represent the negative temperature dependence of the rate constants over a wide temperature range.[17] The fitted rate constants are $(2.9 \pm 0.7) \times 10^{-11} \times (T/298\text{ K})^{(-0.90\pm0.15)}$ cm^3 molecule^{-1} s^{-1} and $(1.1 \pm 0.2) \times 10^{-11} \times (T/298\text{ K})^{(-0.82\pm0.026)}$ cm^3 molecule^{-1} s^{-1} for NH_3 and ND_3, respectively. The primary kinetic isotope effects, defined as the ratio of the rate constants $k(C_2H + NH_3)/k(C_2H + ND_3) = k_{NH_3}/k_{ND_3}$ are 2.1 ± 0.5, 1.7 ± 0.4, and 2.1 ± 0.5 for $T = 104$ K, $T = 165$ K, and $T = 296$ K, respectively. The isotope effect does not show a temperature

dependence in the 104−296 K range within experimental uncertainty.

4. Discussion

4.a. Reaction Mechanism. In the low-pressure limit there are two possible channels for the $C_2H + NH_3$ reaction, which are the hydrogen abstraction reaction, R1, and the addition/elimination reaction, R2. Previous theoretical work on the reverse $NH_2 + C_2H_2$ reaction predicts that there is no activation energy for the R1 channel;[15] unfortunately, there are no theoretical predictions for the R2 channel. The knowledge about the relative importance of R1 and R2 is valuable to understanding in what way the $C_2H + NH_3$ reaction may be important in planetary atmospheres and interstellar media. For example, one of the key questions for the photochemistry of the upper troposphere of Saturn and Jupiter is whether the $C_2H + NH_3$ reaction simply recycles acetylene, which corresponds to R1, or produces larger organonitrogen molecules, which corresponds to R2.

Hydrogen atom abstraction reactions, similar to R1, have been studied extensively, and most details of the mechanisms of these reactions are well understood. What may distinguish this particular hydrogen abstraction reaction from the well-studied cases of hydrogen atom abstraction reactions by halogen atoms or hydroxyl radical is the possibility that the dynamics of this reaction can be influenced by the propensity to form long-lived, relatively strongly bound complexes of the reactants. There are no previous theoretical studies of the potential energy surfaces for the $NH_3\cdots C_2H$ van der Vaals complex. The closest system to a $NH_3\cdots C_2H$ complex that has been studied is the $NH_3\cdots$CO complex.[22] In that study the potential energy surface for the $NH_3\cdots$CO complex has multiple local minima, separated by small barriers. It is possible that the same is true for the $NH_3\cdots C_2H$ van der Waals complex, and the dynamics of the $C_2H + NH_3$ reaction at low collision energies may be complicated by unimolecular dynamics of the relatively long-lived $NH_3\cdots C_2H$ complex, i.e., isomerization between the multiple minima coupled with tunneling.

It is interesting to compare the $C_2H + NH_3$ reaction with the relatively well studied $CN + NH_3$ reaction to gain more insight into the R2 channel for $C_2H + NH_3$.[23] For the $CN + NH_3$ reaction, not only have the rate constants been measured, but also the products of the reaction were detected, which are NH_2 and HCN.[23] On the basis of the products, one might presume that a simple direct hydrogen abstraction channel would be the major channel for the $CN + NH_3$ reaction. This is not the case, however, as theoretical calculations show, and the reaction proceeds via the $NC-NH_3$ complex, which rearranges to give the final products.[23] A similar mechanism is possible for the $C_2H + NH_3$ reaction. However, one has to consider an important difference between the C_2H and CN radicals, which is the directions of the dipole moments of C_2H and CN. For the $CN + NH_3$ reaction, when the CN radical attacks the lone pair on the nitrogen atom, the direction of the CN dipole moment favors an approach of the carbon in CN toward the nitrogen in NH_3; for the $C_2H + NH_3$ reaction, the direction of the C_2H dipole moment is less favorable for this approach, based on simple electrostatics. On the other hand, while the electrostatic interaction dominates the interaction between the reactants at long distances, at the shorter distances the dipole−dipole interaction may not be the dominant contribution to the interaction potential and it is possible that the chemical bonding interaction of the R2 channel reaction may be important for the $C_2H + NH_3$ reaction.

4.b. Kinetic Isotope Effect. There are many factors that can explain the observed kinetic isotope effect for the $C_2H + NH_3$ reaction, such as tunneling, changes in the partition functions of the reactants and activated complexes, changes in the zero point energies, etc. It is difficult to judge the relative importance of these factors without the aid of transition state or reactive scattering calculations. Unfortunately, accurate calculations are not possible since no potential energy surface is available for this reaction.

The mechanism of the $C_2H + NH_3$ reaction involves motion of a hydrogen atom for both the R1 and R2 channels. It has been shown that for many reactions involving motion of a hydrogen atom, the contribution of tunneling to the reaction rate constant can be significant. Similarly, it is possible that tunneling also contributes significantly to the $C_2H + NH_3$ rate constant. Replacing the hydrogen atom with a deuterium atom will decrease the tunneling probability, which could be consistent with the observed decrease in the rate constant. Tunneling may explain some of the observed kinetic isotope effect.

One can also try to explain the observed kinetic isotope effect by using statistical theories of the reaction rate constants. In the classical formulation of transition state theory (TST) the ratio for the kinetic isotope effect is given by the following expression:

$$k_{NH_3}/k_{ND_3} = ((M_{ND_3} + M_{C_2H})/(M_{NH_3} + M_{C_2H}))^{3/2} \times (Z^{rot}_{ND_3}/Z^{rot}_{NH_3})(Z^{rot}_{NH_3\cdots C_2H}/Z^{rot}_{ND_3\cdots C_2H}) \times (Z^{vib}_{ND_3}/Z^{vib}_{NH_3})(Z^{vib}_{NH_3\cdots C_2H}/Z^{vib}_{ND_3\cdots C_2H}) \times (Z^{intermolecular}_{NH_3\cdots C_2H}/Z^{intermolecular}_{ND_3\cdots C_2H}) \times \exp(-\Delta E^{\ddagger}_0/kT) \quad (2)$$

In this expression M_{C_2H}, M_{NH_3}, and M_{ND_3} are the molecular masses of the reactants, Z^{rot} are the rotational partition functions, Z^{vib} are the vibrational partition functions associated with the intramolecular vibrational modes, $Z^{intermolecular}$ are the partition functions associated with the relative motion of the C_2H and NH_3 or ND_3 fragments in the activated complexes and the last factor is due to the change in the zero point energy. While the first three factors in eq 2 can be estimated for an assumed geometry of the activated complex, accurate evaluation of the last two factors in eq 2 is not possible since it requires information about the potential energy surface that is not available. Thus, a definite conclusion about the origin of observed kinetic isotope cannot be made without further work. Nevertheless, eq 2 points out an important detail about the effect of isotopic substitution on the $C_2H + NH_3$ reaction, which is a large increase in the density of states of the reactants upon isotopic substitution of D for H. It could be possible that isotopic substitution does not increase the density of states in the activated complex as much as it increases the density of states in the reactants, and this may explain part of the observed kinetic isotope effect. The increase in the reactant density of states comes mainly from the rotational degrees of freedom, since the isotopic substitution changes all three moments of inertia of ammonia by approximately a factor of 2. In the activated complex, isotopic substitution does not change the moments of inertia as much, and at best it can change only one moment of inertia significantly (by a factor of 2). This best case scenario assumes a prolate near symmetric top geometry of the activated complex, similar to the assumed geometry of the activated complex for the R1 channel. Thus, for the rotational degrees of freedom there is a large increase in the rotational partition

function of the reactants that is not compensated for by a corresponding increase in the rotational partition function of the activated complex. This would lead to a temperature-independent kinetic isotope effect $k_{NH_3}/k_{ND_3} > 1$, consistent with the experiment and would explain the observed kinetic isotope effect if it were not for the fact that the last two factors in eq 2 cannot be estimated. It also should be noted that while a description using classical TST may be too simplistic considering that the $C_2H + NH_3$ reaction does not have a barrier, in other versions of TST such as the statistical adiabatic channel model,[24] an increase in the rotational density of states of the reactants will also lead to $k_{NH_3}/k_{ND_3} > 1$.

For the $C_2H + NH_3$ reaction, explanation of the kinetic isotope effect based only on the change in the zero point energies is inconsistent with the lack of temperature dependence for k_{NH_3}/k_{ND_3}. As can be seen from eq 2, if there is a significant change in $E^{\ddagger}_0$ upon isotopic substitution, then there should be a significant temperature dependence of the kinetic isotope effect through the $\exp(-\Delta E^{\ddagger}_0/kT)$ factor, which is not what is observed experimentally. If a change in the zero point energies is essential for the explanation of the kinetic isotope effect, then there should be some other equally important factors that would cancel the temperature dependence from the $\exp(-\Delta E^{\ddagger}_0/kT)$ factor and make k_{NH_3}/k_{ND_3} temperature independent.

To summarize, in the above discussion some possibilities that can explain the observed kinetic isotope effect are outlined; however, an explanation of the magnitude and the lack of temperature dependence of the observed kinetic isotope effect will have to wait until information about the potential energy surface for this reaction becomes available.

4.c. Negative Temperature Dependence of the Rate Constant. The rate constants for the $C_2H + NH_3/ND_3$ reactions increase with decreasing temperature approximately as $T^{-0.9}$. These experimentally measured temperature dependences of the rate constants can be compared with the predictions of a model where the rate constant is determined by the capture of the reactants by long-range attractive electrostatic forces. In this model, for a given collision energy the reaction cross section is determined by the capture radius. The capture radius is defined by a condition on the impact parameter at which the centrifugal barrier is equal to the potential energy. For the $C_2H + NH_3$ reaction, the long-range interaction between NH_3 and C_2H is dominated by the dipole−dipole interaction, since both reactants have large permanent dipole moments (1.47 D for NH_3 and 0.77 D for C_2H). If the anisotropy of the dipole−dipole interaction is neglected, then the model predicts that the rate constant should depend on the temperature as $T^{-2/3}$. This predicted temperature dependence ($T^{-2/3}$) is relatively close to the observed temperature dependence ($T^{-0.9}$), with the difference being that the observed temperature dependence is stronger than predicted by a capture model. Some of this discrepancy can be explained by the fact that the isotropic dipole−dipole interaction potential used in the model may not approximate the real interaction potential accurately enough. Also, theory explains some of this discrepancy by noting that in barrierless reactions a very strong dependence of the reaction cross sections on the initial internal angular momentum of the reactants is often observed. The observed negative temperature dependence of the rate constants is related to the change in the initial rotational distributions of the reactants with changing temperature. The details of this explanation and some of the references are given in a review of reaction kinetics at very low temperature.[24]

4.d. Comparison to the CN + NH_3 and CH + NH_3 Reactions. It is interesting to compare the results obtained for the $C_2H + NH_3$ reaction to the results obtained for the CN or CH + NH_3 reactions. Reactions of the C_2H, CN, and CH radicals with ammonia are similar in the sense that all three of these reactions can presumably proceed via the hydrogen abstraction mechanism, or via formation of a new CN bond followed by rearrangement and/or elimination of hydrogen atom(s). The reactants in all three reactions have large dipole moments, so the strong attraction between the reactants is another common feature of these three reactions. The dipole moments and polarizabilities of the CN and CH radicals are almost identical, and the value of the dipole moment for the C_2H radical is approximately two times smaller than the dipole moments for the CN and CH radicals. The rate constant for the CN + NH_3 reaction is $(2.77 \pm 0.67) \times 10^{-11} \times (T/298\ \mathrm{K})^{(-1.14\pm0.15)}$ cm^3 molecule^{-1} s^{-1},[16] compared to the rate constant for the $C_2H + NH_3$ reaction $(2.9 \pm 0.7) \times 10^{-11} \times (T/298\ \mathrm{K})^{(-0.90\pm0.15)}$ cm^3 molecule^{-1} s^{-1}. Fortuitously, the rate constants for these two reactions are essentially the same within the experimental uncertainty. The rate constant for the CH + NH_3 reaction is approximately seven times larger than the rate constant for the CN + NH_3 reaction at room temperature and has a negative temperature dependence over the 75 K < T < 300 K temperature range.[17]

The experimentally measured values of all three rate constants for these three reactions do not correlate well with the values that would be obtained from the theoretical model based on capture at long range. The capture model qualitatively explains the negative temperature dependence of the rate constants for all three reactions, but obviously capture of the reactants by attractive forces is only a part of the reaction mechanisms.

The similarity in the experimental data for the CN + NH_3/ND_3 reactions and $C_2H + NH_3/ND_3$ reactions is not limited just to the fact that the rate constants for these two reactions are nearly identical. The kinetic isotope effect, also defined as k_{NH_3}/k_{ND_3} for the CN + NH_3/ND_3 reactions, is nearly identical for the reactions of C_2H and CN with ammonia.[23] On the basis of the results of theoretical calculations, in a combined experimental and theoretical investigation of the CN + NH_3 reaction it was concluded that the kinetic isotope effect for the CN + NH_3/ND_3 can best be explained by assuming that tunneling is very important for this reaction.[23] As was mentioned above, tunneling may also be important for the $C_2H + NH_3$ reaction.

Acknowledgment. The support of this research by the National Aeronautics and Space Administration (Grant NAGS-13339) is gratefully acknowledged. Additional equipment and laboratory facilities were provided by the Department of Energy, supported by the Director, Office of Science, Office of Basic Energy Sciences, U.S. Department of Energy, under Contract No. DE-AC-03-76SF00098. Some equipment was obtained on loan from the National Institute of Standards and Technology.

References and Notes

(1) Strobel, D. F. *Planet. Space Sci.* **1982**, *30*, 839.

(2) Allen, M.; Yung, Y. L.; Gladstone, G. R. *Icarus* **1992**, *100*, 527.

(3) Jackson, W. M.; Bao, Y. H.; Urdahl, R. S. *J. Geophys. Res.-Planets* **1991**, *96*, 17569.

(4) Tucker, K. D.; Kutner, M. L.; Thaddeus, P. *Astrophys. J.* **1974**, *193*, L115.

(5) Hasegawa, T. I.; Kwok, S. *Astrophys. J.* **2001**, *562*, 824.

(6) Markwick, A. J.; Ilgner, M.; Millar, T. J.; Henning, T. *Astron., Astrophys.* **2002**, *385*, 632.

(7) Shaub, W. M.; Bauer, S. H. *Combust. Flame* **1978**, *32*, 35.

(8) Devriendt, K.; Peeters, J. *J. Phys. Chem. A* **1997**, *101*, 2546.

(9) Atreya, S. K.; Pollack, J. B.; Matthews, M. S. *Origin and Evolution of Planetary and Sattellite Atmospheres*; The University of Arizona Press: Tucson, AZ, 1989.
(10) Kaye, J. A.; Strobel, D. F. *Icarus* **1983**, *54*, 417.
(11) Tokunaga, A. T.; Beck, S. C.; Geballe, T. R.; Lacy, J. H.; Serabyn, E. *Icarus* **1981**, *48*, 283.
(12) Weisstein, E. W.; Serabyn, E. *Icarus* **1996**, *123*, 23.
(13) Bagenal, F.; Dowling, T.; McKinnon, W. *Jupiter: The Planet, Satellites and Magnetosphere*; Cambridge University Press: Cambridge, England, 2003.
(14) Hennig, G.; Wagner, G. *Phys. Chem. Chem. Phys.* **1995**, *99*, 989.
(15) Moskaleva, L. V.; Lin, M. C. *J. Phys. Chem. A* **1998**, *102*, 4687.
(16) Sims, I. R.; Queffelec, J. L.; Defrance, A.; Rebrionrowe, C.; Travers, D.; Bocherel, P.; Rowe, B. R.; Smith, I. W. M. *J. Chem. Phys.* **1994**, *100*, 4229.
(17) Bocherel, P.; Herbert, L. B.; Rowe, B. R.; Sims, I. R.; Smith, I. W. M.; Travers, D. *J. Phys. Chem.* **1996**, *100*, 3063.
(18) Lee, S.; Hoobler, R. J.; Leone, S. R. *Rev. Sci. Instrum.* **2000**, *71*, 1816.
(19) Vakhtin, A. B.; Lee, S.; Heard, D. E.; Smith, I. W. M.; Leone, S. R. *J. Phys. Chem. A* **2001**, *105*, 7889.
(20) Murphy, J. E.; Vakhtin, A. B.; Leone, S. R. *Icarus* **2003**, *163*, 175.
(21) Carl, S. A.; Nguyen, H. M. T.; Nguyen, M. T.; Peeters, J. *J. Chem. Phys.* **2003**, *118*, 10996.
(22) Toczylowski, R. R.; Johnson, R. C.; Cybulski, S. M. *J. Mol. Struct.* **2002**, *591*, 77.
(23) Meads, R. F.; Maclagan, R.; Phillips, L. F. *J. Phys. Chem.* **1993**, *97*, 3257.
(24) Smith, I. W. M.; Rowe, B. R. *Acc. Chem. Res.* **2000**, *33*, 261.